EPJ manuscript No.
(will be inserted by the editor)

Investigating the reasons of variability in Si IV and C IV Broad Absorption Line troughs of Quasars

D. Stathopoulos[1,2], E. Lyratzi[1,2], E. Danezis[1], A. Antoniou[1], and D. Tzimeas[1]

[1] National and Kapodistrian University of Athens, Faculty of Physics, Panepistimioupoli, Zographou 157 84, Athens, Greece
[2] Eugenides Foundation, 387 Syngrou Av., 175 64, Athens, Greece

Received: date / Revised version: date

Abstract. In this paper we analyze the C IV and Si IV broad absorption troughs of two BALQSOs (J101056.69+355833.3, J114548.38+393746.6) to the individual components they consist of. By analyzing a BAL trough to its components we have the advantage to study the variations of the individual absorbing systems in the line of sight and not just the variations of the whole absorption trough or the variations of selected portions of BAL troughs exhibiting changes. We find that the velocity shifts and FWHMs (Full Width at Half Maximum) of the individual components do not vary between an interval of six years. All variable components show changes in the optical depths at line centers which are manifested as variations in the EW (Equivalent Width) of the components. In both BALQSOs, over corresponding velocities, Si IV has higher incidence of variability than C IV. From our analysis, evidence is in favour of different covering fractions between C IV and Si IV. Finally, although most of our results favour the crossing cloud scenario as the cause of variability, there is also strong piece of evidence indicating changing ionization as the source of variability. Thus, a mixed situation where both physical mechanisms contribute to BAL variability is the most possible scenario.

PACS. 95.75.Fg Spectroscopy – 98.54.Aj Quasars – 78.40.-q Absorption spectra: ultraviolet – 98.62.Ra Quasar absorption and emission-line systems

1 Introduction

Approximately 20 percent of the total quasar population exhibit Broad Absorption Lines (BALs) in the UV region of the electromagnetic spectrum [1,2]. BALs are usually blueshifted with respect to the corresponding emission lines though there are cases that redshifted absorption has been observed (see [3]). As a result, BALs are the prominent signatures of accretion disk outflows observed in quasar spectra.

BALs are complex and unusually broad absorption troughs which appear remarkably smooth in high resolution spectra. The characteristics of BALs span a wide range in terms of width, velocity shift, level of ionization, strength of absorption and structure of absorption trough. BALs are defined as absorption troughs with velocity widths > 2000 km s^{-1} at depths $> 10\%$ below the continuum [4]. Outflow velocities range from $0-5000$ km s^{-1} up to $10000-30000$ km s^{-1}, while extreme cases of 60000 km s^{-1} have been observed [5]. The structure of absorption troughs can be very smooth, exhibiting P-Cygni like profiles, where single trough absorption which sets in near zero outflow velocity is observed [6]. On the other hand, absorption troughs can be very broken up [6]. There are also cases where multiple trough absorption which sets in near zero outflow velocity is observed. Finally, there are BAL quasars that exhibit detached troughs from the emission peak which do not set in until the outflow reaches a velocity of $3000-5000$ km s^{-1}. The properties of BAL material in phase space are uncertain. One opinion is that BALs are the product of a smooth continuous flow (e.g. [7, 8]) with the intensity depending on optical depth effects (complete source coverage).

On the other hand, it is believed that BALs are due to a flow of many individual substructures in the wind called density enhancements or clumps or clouds, indicating that accretion disc outflows are clumpy (e.g. [9–19]).

Takeuchi, Ohsuga & Mineshige [15], performing global radiation-MHD simulations of supercritical accretion flows onto black holes, found that the outflows associated with supercritical (or super Eddington) accretion flows have a clumpy structure above heights of ~ 250 r$_\mathrm{S}$ (with r$_\mathrm{S}$ being the Schwarzschild radius). The typical clump size is ~ 10 r$_\mathrm{S}$, which corresponds to about one optical depth, and their shapes are slightly elongated along the outflow direction. They also found that the most plausible cause of clump formation is the Rayleigh-Taylor instability, since the clumpy structure appears in the layer where the upward radiation is superior in force to the downward gravity. Furthermore, a radiation-hydrodynamic instability may also help to form clumps of one optical depth.

Recent 2D simulations by Waters & Proga [20] reveal that the long term evolution of a two-phase medium (hypothetical cloud confining medium proposed by Mathews [21] and studied extensively by Krolik, McKee & Tarter [22] - the main idea is of two distinct components, in pressure equilibrium but very different temperature, both heated by the same central source. The gas exposed to the radiation field of a quasar must be in one of two forms: photoionized gas at $\sim 10^4$ K, which produces optical and UV emission lines, or hot gas at $T \sim 10^8$ K. The hot phase gas produces the required confinement and the long life of line emitting clouds) in the Broad Line Region (BLR) is a highly turbulent flow that is conducive to continuous cloud production. They also found that cloud production can be maintained because the turbulence supplies perturbations that continually trigger the thermal instability.

To conclude, the "cloud" scenario seems a more plausible explanation for the formation of BAL troughs than the smooth continuous flow interpretation, due to the following reasons:

- BAL trough profiles are complex and cannot be simulated by a single distribution (Gauss, Lorentz, Voigt etc).
- From a theoretical point of view, both Takeuchi et al. [15] and Waters & Proga [20] predict clumpy outflows due to instabilities in the highly turbulent medium.
- Misawa et al.[17] by observing multiple sight lines with the aid of strong gravitational lensing managed to resolve the clumpy structure of the outflow winds in the quasar J1029 +2623. Through their observations they rejected the hypothesis of a smooth homogeneous outflow and concluded to complex small structures inside the outflow from the galactic nucleus. They proposed two different structures for the clumpy outflow: (a) small gas clouds close to the flux source and (b) filamentary (or sheet-like) structure made of multiple clumpy gas clouds.

Although accretion disk outflows are so prominent and ubiquitous, their basic physical conditions, acceleration mechanism(s), location and three dimensional structures are not well understood. Absorption line variability is a very useful tool able to provide insights into the structure, dynamics and kinematics of the powerful outflows. In the case of BALQSOs, line variability is commonly attributed to changes in the absorption strength (e.g. [24–33]) and/or appearance, disappearance of absorption troughs ([14,34–37]). In more detail, the variability of absorption troughs is attributed to one of the following reasons: i) changes in the ionization state as a function of velocity (changes in the ionization state of the gas result in change on the column density of the absorbing ion, e.g. [38]), ii) changes in the acceleration profile and/or geometry of the outflow due to change in the driving force or mass-loss rate, iii) line of sight acceleration of a shell of material from a continual flow and iv) transverse motion of the absorbing cloud(s) relative to the line of sight [27,36,39–41]. However the two most dominant mechanisms are supposed to be the movement of substructures in the flow (individual clouds) along our line of sight and changes in ionization [26,27,42–45]. However, Capellupo et al. [30] argue that the actual situation may be a complex mixture of changing ionization and cloud movements.

Coordinated variabilities between absorption regions at different velocities in individual quasars seem to favor changing ionization of the outflowing gas as the cause of the observed BAL variability [30]. So, when there is variability in different velocity intervals within the same BAL or within multiple BALs in the same quasar, the changes almost always occur in the same sense and the most likely explanation for this is a global change in ionization [30]. Another argument favoring ionization changes is that changes in BAL strength are not necessarily monotonic [46]. One further piece of evidence is the correlation between continuum variability and BAL variations which is found in certain individual quasars [42]. In general, a change in ionization should cause more global changes, rather than changes in small, discrete velocity intervals.

On the other hand, variability in limited portions of broad troughs fits naturally in a scenario where movements of individual clouds or substructures in the flow, across our lines-of-sight, cause the absorption to vary [30]. Gibson et al. [44] reported variability over narrow velocity ranges within troughs across several different ions at the same velocity, which seems to favor the movement of absorbing clouds across the line of sight (hence changing the covering fraction), as the dominant mechanism of BAL variability. Another strong piece of evidence that supports the cloud picture is that in certain BALs, one portion of the BAL strengthens, while another weakens within the same quasar. This can be explained in a moving cloud scenario, for it is possible for clouds at different velocities to enter/leave our line-of-sight at different times [30]. Finally, there are studies that show no correlation between continuum variability and BAL variations, a fact that favors the cloud crossing scenario [27,44,47].

In the case of individual quasars, Hamann et al. [24] observed intrinsic N V, Si IV and C IV absorbers varying in unison over $\lesssim 4$ months in the QSO Q2343+125. From their study, they found that the absorbers cover $\lesssim 20\%$ of the continuum while there were piece of evidence that variation was due to changes in covering fraction. Finally, Misawa et al. [48] observed a mini-BAL, in the QSO HS 1603+3820, which exhibited significant substructure that varied in concert.

Strong evidence of covering fraction changes comes from changes in the fractional EW ($\Delta EW/ < EW >$) in all ions in the outflow assuming that the crossing clouds responsible for variability have a similar ionization state to the bulk of the outflow [44]. This is true since such variability depends on changes in the total column of absorbing gas along the line-of-sight without any changes in the relative ion populations [44].

Usually, BAL variability studies are performed in two ways:

1. By measuring the variability of the fractional EW of the whole absorption trough [27,46,49]. Wildy, Goad & Allen [50] follow the same method but instead of using the modelled continuum EW they use a modi-

fied EW. However, studying the variation of the whole absorption trough does not reflect the variation of the properties of the physical structures that create the observed absorption.

2. By studying the variation within portions of a trough, instead of using equivalent width measurements of the whole absorption trough [41,44]. Both studies identify velocity intervals with a width of at least 1200 km s^{-1} that varied. Filiz Ak et al. [32] select BAL troughs showing significant EW variations. Then in order to determine the regions in each BAL trough where a variation has occurred they set a criterion (see Eq. 5 in [32]), which has to be satisfied for at least five consecutive data points. This requirement allows detection of variable regions wider than ≈ 275 km s^{-1}. He et al. [51] follow the same method as Filiz Ak et al. [32] but their velocity intervals are 774 km s^{-1}.

At this point we need to mention that EW measurements of wide troughs are less sensitive to strength changes in narrow portions of the trough or to changes in which one part of a BAL weakens, while another part strengthens. As for the variations within portions of BAL troughs, they depend on the number of consecutive data points i.e. the width of the regions one measures variability. The criterion of Filiz Ak et al. [32] allows detection of variable regions wider than ≈ 275 km s^{-1}, and as they point out using a smaller number of consecutive data points as the requirement may cause non-physical observational errors to be indistinguishable from the variable regions of BAL troughs. On the other hand, requiring a larger number of consecutive data points will cause non-detection of narrow variable regions. However, as mentioned earlier Capellupo et al. [41] and Gibson et al. [44] use 1200 km s^{-1} interval while He et al. [51] use 774 km s^{-1} intervals.

However, both cases, i.e. studying the variation of the whole absorption trough and studying independently the variation of parts of the absorption defined as described above, have a disadvantage. The variation measured in these ways does not correspond to the variation of the properties of the physical structures of the BAL QSOs environment that create the observed absorption.

According to GR model [11,52–55] and the physical model and multicomponent analysis method proposed by Stathopoulos et al. [18] the observed BAL troughs are not studied as unique formations. On the contrary, the great advantage of the model is that the observed BAL profiles can be analyzed to its uniquely determined components so each BAL component can be studied independently. This means that each BAL trough is not studied as a whole, but in parts. However, these parts are not arbitrarily selected, but each one of them is an actual absorption component which is created by a real physical structure (cloud) in the BALQSO environment. The variability of the absorption components of the BAL troughs, which is measured in this way, corresponds to the variation of the properties of the physical structures of the BAL QSO environment that create the observed absorption. Besides that, GR model ensures the uniqueness of the number of BAL components as well as the uniqueness of the calculated values of the physical parameters (radial velocity of the clouds, the FWHM, the optical depth, the equivalent width etc), through specific and strong criteria that apply in the case of resonance lines (for a more detailed analysis see [18]).

The aim of this work is to study the variability of BAL troughs and to investigate the mechanisms responsible for causing this variability. To achieve this goal we use GR model [11,52–55] and the multicomponent analysis method proposed by Stathopoulos et al.[18]. We apply the model and method in Si IV and C IV broad absorption trough in the case of two BAL quasars (SDSS J101056.69+355833.3 and SDSS J114548.38+393746.6).

2 Method of analysis

In contrast to most BAL variability studies which study either the variability of the whole observed BAL trough or the variation within portions of a trough, we introduce a different approach. Using the model proposed by Danezis et al. [52–54], Lyratzi et al. [11,55], and the fitting criteria proposed by Stathopoulos et al. [18] we can analyze each BAL trough to the uniquely determined components that it consist of and we study the variability of each individual component. As a result we can study the variability of the physical parameters (FWHM, optical depth, equivalent width, radial velocity) that describe the individual structures, in the outflow, we call clouds.

2.1 Mathematical Expression of the Model and the Fitting Process

The mathematical model is built on the basis that the BALR/BELR consists of a number of absorbing/emitting clouds that intercept the line of sight towards the central regions of the QSO that produce the continuum radiation [55]. The observed BALs/BELs are the synthesis of absorption/emission components produced by these clouds. So, in order to conclude to a mathematical function (interpolation polynomial), that can simulate the complex BAL/BEL profiles produced by clouds, Danezis et al. [52] solved the radiative transfer equation for such a complex plasma region. The final equation (interpolation polynomial) derived by the solution of radiative transfer is:

$$I_\lambda = \left[I_{\lambda 0} \prod_i \exp\{-L_i \xi_i\} + \sum_j S_{\lambda e j} \left(1 - \exp\{-L_{ej}\xi_{ej}\}\right) \right] \prod_g \exp\{-L_g \xi_g\} \quad (1)$$

where:
i: is the number of absorbing clouds that cover the continuum (fully or partially), in the line of sight,
j: is the number of emitting clouds in the line of sight,
g: is the number of additional absorbing clouds that may cover the i absorbing clouds as well as the j emitting

clouds,
$I_{\lambda 0}$: is the initial radiation intensity,
$\prod_i \exp\{-L_i\xi_i\}$: is the factor that describes the synthesis of absorption components produced by i clouds,
$\sum_j S_{\lambda_{ej}}(1-exp(L_{ej}\xi_{ej}))$: is the factor that describes the summation of emission components produced by j clouds,
$\prod_g \exp\{-L_g\xi_g\}$: is the factor that describes absorbing clouds that obscure both the i absorbing as well as the j emitting clouds,
L_i, L_{ej}, L_g: are the distribution functions of the absorption coefficients $k_{\lambda i}$, $k_{\lambda ej}$, $k_{\lambda g}$,
$k_{\lambda i}$: is the absorption coefficient of the i^{th} cloud in the line of sight,
$k_{\lambda ej}$: is the absorption coefficient of the j^{th} emission cloud in the line of sight,
$k_{\lambda g}$: is the absorption coefficient of the additional absorbing clouds that may cover the i and j clouds in the line of sight,
ξ: is the optical depth (τ_0) at the center of the spectral line,
$S_{\lambda ej}$: is the source function, that is constant during one observation.

The geometry of the model is included in the factors "L" of Eq. (1) [53,55]. After investigating a number of geometries we concluded that the best fit of absorption/emission lines is accomplished if the geometry is spherical [56–61]. Apart from the geometry, the parameters "L" can take the expression of one of the following distributions, according to the physical conditions we like to describe. So "L" can take the form of either Gauss (random motions - thermal and non thermal), or Lorentz (pressure), or Voigt (random motions and pressure), or Rotation (rotation of a region around its own center, [52, 53]) or Gauss - Rotation (random motions and rotation of a region around its own center [52,53]).

During the fitting process we use Eq. (1) independently for every component of a doublet. For example in the case of C IV $\lambda\lambda$ 1548.187, 1550.772 Å resonance lines, we apply Eq. (1) twice, once for the 1548.187 Å (blue) and once for the 1550.772 Å (red) component of the doublet. By applying Eq. (1) twice we get two sets of lines. The first one contains all the blue components of C IV doublet (in Fig. 2 in the case of J101056.69+355833.3, there are 9 blue absorption components), while the second one contains all the red components of C IV doublet (in Fig. 2, there are 9 red absorption components). Having these two sets of lines we then synthesize them to get the best fit. In the case of absorption lines we use Gauss distribution while in the case of emission lines we use Voigt distribution. We point out that after the continuum fit we fit the broad emission lines (see Fig. 2).

Furthermore when fitting, we use two sets of criteria (for more details see [18], §3) which are applied to resonance lines which are studied in this paper, that not only provide the best fit but also ensure that the number of components and the values of the parameters used are uniquely determined. As mentioned above the final mathematical function that we interpolate in a spectral region is the synthesis of as many functions (Eq.1) as the lines under study (e.g. for S IV 13913.755, 1402.77 Å we combine two functions, one for the blue line and one for the red line, where the first function describes the synthesis of all the 1393.755 Å components and the second describes all the 1402.77 Å components).

In this work we study the C IV and Si IV resonance lines in the case of two spectra taken at different epochs for two BAL QSOs.

2.2 Physical Model

In order to provide a clearer picture of the physical structure of clouds, as we consider it, we briefly describe the physical model proposed by Stathopoulos et al. [18]. BALs consist of a series of absorption components produced by density enhancements called clouds. Clouds are clusters of subunits called cloud elements or cloudlets (cloud elements-regions II, figure 1 in [18]). To avoid confusion, we will always refer to the larger, more distinct structures as "clouds" (Regions I, figure 1, in [18]) and the smaller structures as "cloud elements" or cloudlets. We borrow the term "cloud elements" from Bottorff & Ferland [23], who assume that each BLR cloud is a collection of overlapping constant density clumps and these smallest clumps are called cloud elements. According to Stathopoulos et al. [18] each cloudlet produces an absorption line the width of which depends on thermal and microturbulent motions of ions inside the cloudlet. The synthesis of all these cloudlet lines that are very close in velocity space and overlap, produce a broad component corresponding to a cloud. So the relatively broad components we use in our fits correspond to clouds. The synthesis of the lines, produced by clouds, form the broad absorption troughs observed in BALQSO spectra. We point out that the so called clouds are not pre-existing structures accelerated by radiation pressure but are structures formed in the outflow as described by Takeuchi, Ohsuga & Mineshige [15] or Waters & Proga [20] who predict that BALQSO outflows are clumpy.

3 Observations and Data Reduction

The spectra we study are taken from Sloan Digital Sky Survey (SDSS) DR10 catalogue. In Table 1 we give the name of the BAL QSO in the first column, the plate, Modified Julian Date (MJD) and fibre are given in the second column, the redshift of each BAL QSO is given in the third column and in the last column we give the spectral index of the power law continuum. In Fig. 1 we give the two epoch spectra of J101056.69+355833.3 and J114548.38+393746.6. With black thick line we denote the BOSS spectrum while with green thin line we denote the SDSS spectrum. Both BALQSOs present variations in both C IV and Si IV broad absorption troughs.

Before fitting the spectra we use the following methods for the correction of the galactic extinction and the continuum fit. We also present the method of error analysis.

Table 1.

Name	plate-MJD-fiber	Redshift	α
J101056.69+355833.3 (BOSS)	4568-55600-0440	2.3010 (Wildy, Goad & Allen [50])	-1.52±0.04
J101056.69+355833.3 (SDSS)	1951-53389-0579	2.3010 (Wildy, Goad & Allen [50])	-1.90±0.05
J114548.38+393746.6 (BOSS)	4654-55659-0856	3.1245 (Filiz Ak et al. [32])	-1.34±0.05
J114548.38+393746.6 (SDSS)	1997-53442-0450	3.1245 (Filiz Ak et al. [32])	-1.64±0.07

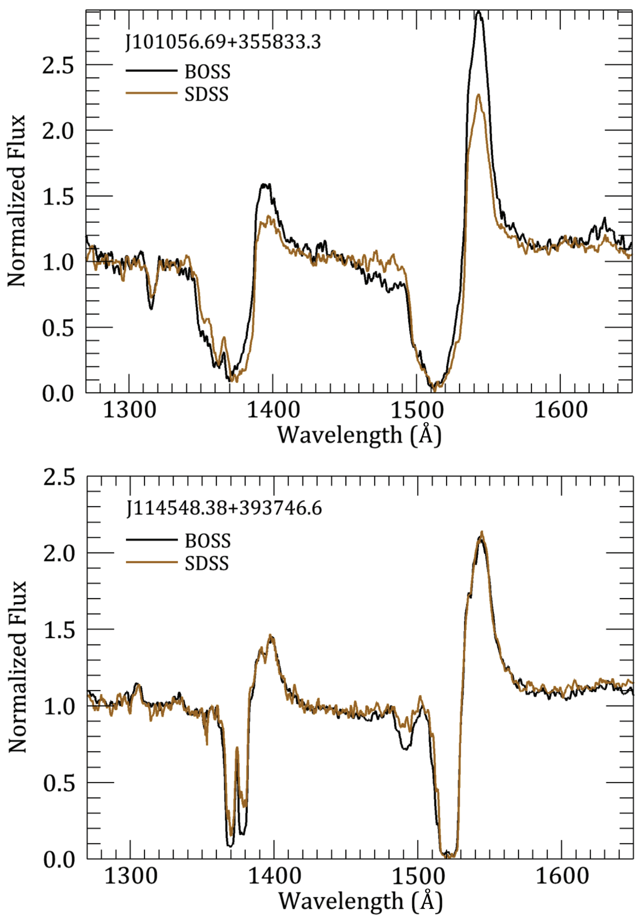

Fig. 1. Top: Comparison of the two different spectra of J101056.69+355833.3. Bottom: Comparison of the two different spectra of J114548.38+393746.6.

3.1 Derredening

We correct both spectra for galactic extinction using the reddening curve of Fitzpatrick & Massa [62] with $R_V = 3.1$. We obtain E(B - V) from the NASA Extragalactic Database (NED), which uses the dust maps of Schlegel et al. [63].

3.2 Continuum Fit

For the continuum we fit a power law model to a set of continuum windows (1290-1300 Å, 1445-1465 Å, 1685-1715Å, 1965-2000 Å) free of strong emission lines using the Levenberg - Marquardt minimization process. For the power law continuum we use:

$$F_\lambda = F_{2000} \times \left(\frac{\lambda}{2000}\right)^\alpha \tag{2}$$

The error for the power-law continuum at the wavelength of λ by error propagation is:

$$\delta(F_{con}) = F_\lambda \sqrt{\left(\frac{\delta(F_{2000})}{F_{2000}}\right)^2 + (ln\lambda - ln2000)^2 \delta\alpha^2} \tag{3}$$

where the errors of $\delta(F_{2000})$ and $\delta\alpha$ are given in the power law fitting.

The values of the spectral indices (α) and their corresponding errors are given in the last column of Table 1.

3.3 Error Analysis

The uncertainties of absorption line fitting parameters are estimated by adding Gaussian noise to the best fits. The width of the Gaussian at each pixel equals the flux uncertainty at that pixel. For each best fit, we produce 60 noisy spectra and fit each one of them in the same manner we fit the original spectrum. The uncertainty of each spectral parameter is then measured from its distribution. The error of a spectral parameter is then calculated as the RMS of 60 fitting results.

The true FWHM is determined considering the instrumental width of the spectrograph, by using the following equation [64]:

$$FWHM_{obs}^2 = FWHM_{true}^2 + (1+z)^{-2} FWHM_{inst}^2 \tag{4}$$

where the instrumental broadening ($FWHM_{inst}$) is observed frame while the observed ($FWHM_{obs}$) and true ($FWHM_{true}$) full width at half maximum are rest-frame. For most SDSS fibers this effect is between forty and ninety kilometers per second.

The mean uncertainty in velocity shifts is $\sim$ 200 km s^{-1}. The mean uncertainties for FWHM, EW, τ are $\sim$ 12%, 10% and 18% respectively.

4 Results

4.1 The case study: BALs of J101056.69+355833.3 and J114548.38+393746.6

In order to study the variability of C IV and Si IV resonance lines of the two BALQSOs of Table 1, we applied the GR model to two spectra of each BALQSO, taken at different epochs. By achieving the best fits we managed to analyse the C IV and Si IV BALs to their components. In Fig. 2 we give, as an example, the best fits of the C IV and Si IV spectral regions of J101056.69+355833.3 for the BOSS spectrum taken on 08/02/2011. The black dotted line denotes the observed spectrum while black, thick solid line corresponds to the best fit. With blue thin solid line we denote the shorter wavelength member of a doublet (blue: 1548.187 Å for C IV and 1393.755 Å for Si IV) while with the red dashed line we denote the longer wavelength member of a doublet (red: 1550.772 Å for C IV and 1402.77 Å for Si IV). Below each fit we present a panel with the residual, which appears in green thin line.

Having analysed the BAL troughs to the components they consist of we calculate the Full Width at Half Maximum (FWHM), the optical depth at line center (τ_0) and the Equivalent Width (EW) of each one of the BAL components, as well as the radial velocity (V_{rad}) of the regions that create the components. The values of the calculated parameters for both QSOs on both epochs are presented on Tables 2 and 3.

The BAL troughs of Si IV and C IV of J101056.69+355833.3 are decomposed into 9 different doublets, which means 9 different absorption systems in the line of sight. These systems are characterized by velocities ranging from ~ -3900 km s^{-1} to ~ -12500 km s^{-1}. In the case of J114548.38+393746.6 the BAL troughs of Si IV and C IV are analysed into 10 different doublets, i.e. 10 absorption systems in the line of sight. Their velocities range from ~ -1800 km s^{-1} to ~ -7700 km s^{-1}.

In Tables 2 and 3 one can observe that none of the BAL quasars presents variations in the components' radial velocities between the two epochs. This applies both to Si IV and C IV. In fact, there are indeed small variations between the values of the radial velocities among the two epochs but these variations are smaller than 200 km s^{-1} which is the error in the calculation of V_{rad}. So none of the components is considered to have variable radial velocity. Furthermore, as it is evident from Tables 2 and 3 in both BALQSOs we do not observe any changes in the widths (FWHM) of individual components between two epochs. This applies to Si IV and C IV.

For the purpose of determining which components exhibit variations in line strength, between two different epochs, we define a measurement of the deviation between two components, in units of σ using the following equation [32]:

$$N_\sigma(\lambda) = \frac{f_2 - f_1}{\sqrt{\sigma_1^2 + \sigma_2^2}} \tag{5}$$

where f_1, f_2 are the normalized flux densities of the components under comparison that are calculated through the proposed model and σ_1, σ_2 are the normalized flux density standard deviations at wavelength λ (both σ_1 and σ_2 include observational errors and uncertainties from the fitting process). We identify variable components of BAL troughs, when an absorption component is detected with $N_\sigma \geq 1$ or $N_\sigma \leq -1$ in the core of the component. The values of N_σ for Si IV and C IV for both BALQSOs are given in Table 4 where one can observe which components of SI IV and C IV BAL troughs exhibit variations. All variable Si IV and C IV components of both BALQSOs are also evident in FIg.3. In Fig. 3 we plot only the blue members of Si IV and C IV doublets as the red members exhibit the same trends as the blue ones. In the figure we denote all variable components with filled squares and circles.

We note that in the BAL trough of Si IV in J114548.38+393746.6, the blue member of the 9th doublet (at ~ -6870 km s^{-1}) exhibits variation between the two epoch spectra, with $N_\sigma(\lambda) = -1.08$. In contrast, the red member of the doublet (at the same velocity shift) does not exhibit variation between the two epochs, with $N_\sigma(\lambda) = 0$. However, the total equivalent widths $EW_{(b+r)}$ (BOSS) and $EW_{(b+r)}$ (SDSS) practically do not vary, presenting a variation of $\sim 10\%$. As a result we do not consider this doublet variable. We make the assumption that this relative change in depths between the blue and red member of the doublet is a geometrical effect, i.e. a change in covering fraction.

We point out that all variable components exhibit variations in their optical depths τ_0 which are also manifested as changes in the equivalent widths. As long as all of the components maintain constant FWHMs between two epochs, the variations in EW follow exactly the variations of optical depths.

5 Discussion

Due to the strict criteria [18] we apply during the fitting process we are able not only to distinguish the individual components that compose the final profiles but also calculate the values of the physical parameters of each individual component. Thus we are able to compare individual components between different epochs and investigate the variability of individual structures in the outflow.

As mentioned above, in all studied components, in both BALQSO, we did not observe any changes in velocity shifts so there is no evidence for acceleration or de acceleration of the absorbing systems in the line of sight.

In both BALQSO spectra Si IV exhibits more variable components than C IV. More specifically, in J101056.69+355833.3 from the 9 absorption components of C IV only 2 show variation in EW, while in Si IV from the 9 absorption components there are 6 components that have variable EW. In the case of J114548.38+393746.6 from 10 absorption components of C IV 2 exhibit variation in EW while from the 10 absorption components of S IV 5 of them show variations in EW. The comparisons show

Table 2. Radial velocity (V_{rad}) in km s^{-1}, FWHM in km s^{-1}, optical depth at line center (τ_0) and equivalent width (EW) in Å for the 9 components of the blue (b) and the red (r) lines of the C IV and Si IV doublets for the spectrum of J101056.69+355833.3, taken on 19/01/2005 and 08/02/2011

J101056.69+355833.3 (19/01/2005)								
C IV Component	$V_{rad}(b)$	FWHM(b)	τ_0(b)	EW(b)	$V_{rad}(r)$	FWHM(r)	τ_0(r)	EW(r)
1	-3800	1500	0.66	4.39	-3800	1500	0.66	4.39
2	-4750	1450	0.21	1.57	-4740	1450	0.21	1.57
3	-5550	1500	0.70	4.59	-5530	1500	0.35	2.57
4	-6340	1370	0.50	3.18	-6310	1370	0.25	1.72
5	-7330	1370	0.72	4.27	-7340	1370	0.40	2.63
6	-8270	1370	0.42	2.74	-8260	1370	0.27	1.85
7	-9130	1370	0.27	1.87	-9110	1370	0.27	1.85
8	-10070	1460	0.35	2.49	-10050	1460	0.35	2.49
9	-12450	2380	0.05	0.64	-12440	2390	0.03	0.39
Si IV Component	$V_{rad}(b)$	FWHM(b)	τ_0(b)	EW(b)	$V_{rad}(r)$	FWHM(r)	τ_0(r)	EW(r)
1	-3830	1190	0.87	4.27	-3810	1190	0.87	4.27
2	-4710	1000	0.98	3.94	-4590	1000	0.98	3.94
3	-5580	910	0.44	1.90	-5530	910	0.22	1.02
4	-6500	910	0.33	1.48	-6460	910	0.16	0.76
5	-7410	960	0.32	1.51	-7360	960	0.18	0.89
6	-8270	910	0.31	1.40	-8240	910	0.20	0.94
7	-9150	960	0.53	2.33	-9070	960	0.52	2.30
8	-10040	910	0.13	0.62	-10000	910	0.13	0.62
9	-12430	1600	0.09	0.77	-12390	1600	0.06	0.52
J101056.69+355833.3 (08/02/2011)								
C IV Component	$V_{rad}(b)$	FWHM(b)	τ_0(b)	EW(b)	$V_{rad}(r)$	FWHM(r)	τ_0(r)	EW(r)
1	-4000	1550	0.46	3.36	-3990	1550	0.46	3.36
2	-4780	1380	0.19	1.34	-4800	1380	0.18	1.27
3	-5600	1450	0.57	3.54	-5600	1450	0.31	2.24
4	-6300	1370	0.50	3.18	-6290	1370	0.30	2.04
5	-7370	1370	0.57	3.54	-7360	1370	0.52	3.28
6	-8270	1370	0.40	2.63	-8260	1370	0.35	2.34
7	-9130	1370	0.24	1.66	-9110	1370	0.24	1.66
8	-10070	1460	0.41	2.86	-10050	1460	0.36	2.55
9	-12460	2390	0.15	1.87	-12440	2400	0.10	1.27
Si IV Component	$V_{rad}(b)$	FWHM(b)	τ_0(b)	EW(b)	$V_{rad}(r)$	FWHM(r)	τ_0(r)	EW(r)
1	-4000	1550	0.46	3.36	-3990	1550	0.46	3.36
2	-4780	1380	0.19	1.34	-4800	1380	0.18	1.27
3	-5600	1450	0.57	3.54	-5600	1450	0.31	2.24
4	-6300	1370	0.50	3.18	-6290	1370	0.30	2.04
5	-7370	1370	0.57	3.54	-7360	1370	0.52	3.28
6	-8270	1370	0.40	2.63	-8260	1370	0.35	2.34
7	-9130	1370	0.24	1.66	-9110	1370	0.24	1.66
8	-10070	1460	0.41	2.86	-10050	1460	0.36	2.55
9	-12460	2390	0.15	1.87	-12440	2400	0.10	1.27

Table 3. Radial velocity (V_{rad}) in km s^{-1}, FWHM in km s^{-1}, optical depth at line center (τ_0) and equivalent width (EW) in Å for the 9 components of the blue (b) and the red (r) lines of the C IV and Si IV doublets for the spectrum of J114548.38+393746.6, taken on 13/03/2005 and 08/04/2011

J114548.38+393746.6 (13/03/2005)								
C IV Component	$V_{rad}(b)$	FWHM(b)	τ_0(b)	EW(b)	$V_{rad}(r)$	FWHM(r)	τ_0(r)	EW(r)
1	-1850	890	0.12	0.56	-1840	890	0.10	0.47
2	-2960	500	0.14	0.37	-2920	500	0.12	0.32
3	-4290	730	1.00	2.91	-4290	730	0.88	2.64
4	-4820	680	1.11	2.93	-4800	680	0.88	2.49
5	-5280	630	0.41	1.25	-5270	630	0.38	1.17
6	-5730	570	0.27	0.77	-5720	570	0.20	0.58
7	-6010	820	1.25	3.81	-5960	820	0.82	2.83
8	-6440	570	0.14	0.42	-6430	570	0.12	0.36
9	-6880	540	0.73	1.73	-6870	540	0.61	1.50
10	-7650	500	0.35	0.86	-7640	500	0.22	0.56
Si IV Component	$V_{rad}(b)$	FWHM(b)	τ_0(b)	EW(b)	$V_{rad}(r)$	FWHM(r)	τ_0(r)	EW(r)
1	-1790	590	0.13	0.40	-1870	590	0.12	0.37
2	-2940	330	0.08	0.14	-2920	330	0.07	0.12
3	-4340	450	0.15	0.36	-4310	450	0.11	0.27
4	-4860	400	1.15	1.80	-4830	400	1.15	1.80
5	-5280	400	1.60	2.22	-5290	400	1.14	1.79
6	-5780	360	0.80	1.23	-5740	360	0.80	1.23
7	-5960	540	0.29	0.79	-5920	540	0.20	0.56
8	-6440	360	0.13	0.25	-6400	360	0.11	0.21
9	-6900	360	0.13	0.25	-6830	360	0.10	0.19
10	-7670	360	0.11	0.21	-7600	360	0.10	0.19
J114548.38+393746.6 (08/04/2011)								
C IV Component	$V_{rad}(b)$	FWHM(b)	τ_0(b)	EW(b)	$V_{rad}(r)$	FWHM(r)	τ_0(r)	EW(r)
1	-1850	890	0.13	0.61	-1840	890	0.11	0.52
2	-2960	500	0.14	0.37	-2920	500	0.12	0.32
3	-4290	730	1.02	2.95	-4290	730	0.96	2.82
4	-4820	680	1.12	2.95	-4800	680	0.81	2.34
5	-5280	630	0.44	1.33	-5270	630	0.38	1.17
6	-5730	570	0.27	0.77	-5700	570	0.20	0.58
7	-6010	820	1.12	3.54	-5960	820	0.81	2.80
8	-6440	570	0.14	0.42	-6430	570	0.13	0.39
9	-6840	540	0.98	2.15	-6870	540	0.71	1.69
10	-7650	500	0.65	1.44	-7640	500	0.47	1.11
Si IV Component	$V_{rad}(b)$	FWHM(b)	τ_0(b)	EW(b)	$V_{rad}(r)$	FWHM(r)	τ_0(r)	EW(r)
1	-1790	590	0.18	0.55	-1870	590	0.09	0.28
2	-2980	330	0.08	0.14	-2990	330	0.07	0.12
3	-4340	450	0.15	0.36	-4310	450	0.11	0.27
4	-4860	400	1.42	2.07	-4830	400	1.38	2.03
5	-5300	420	2.24	2.78	-5290	420	2.17	2.73
6	-5760	420	1.37	2.11	-5720	420	1.37	2.11
7	-5960	540	0.42	1.10	-5900	540	0.33	0.89
8	-6440	360	0.25	0.46	-6400	360	0.19	0.36
9	-6920	400	0.17	0.36	-6860	400	0.10	0.22
10	-7720	360	0.10	0.19	-7640	360	0.09	0.17

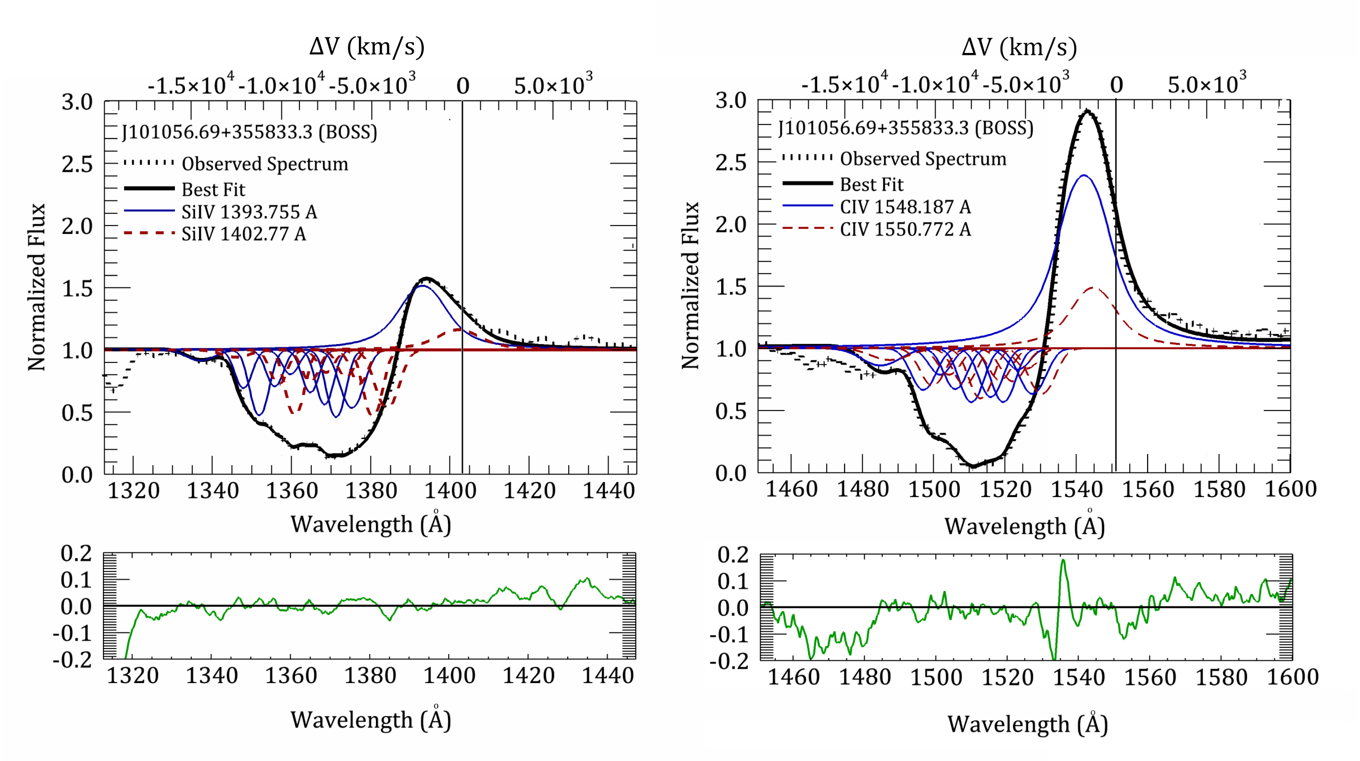

Fig. 2. Best fits of the C IV and Si IV spectral regions of J101056.69+355833.3 for the spectra taken on 19/01/2005 (SDSS) and 08/02/2011 (BOSS). The black dotted line denotes the observed spectrum while black, thick solid line corresponds to the best fit. With blue thin solid line we denote the shorter wavelength member of a doublet (blue: 1548.187 Å for C IV 1393.755 Å and for Si IV) while with the red dashed line we denote the longer wavelength member of a doublet (red: 1550.772 Å for C IV and 1402.77 Å for Si IV). Below each fit we present a panel with the residual, which appears in green thin line.

that over corresponding velocities Si IV has higher incidence of variability than C IV. This result is in agreement with the findings of Capellupo et al. [30] and Wildy, Goad & Allen [50]) and is usually interpreted in terms of line strengths, as the Si IV BALs are generally weaker than C IV BALs and weaker lines tend to be more variable [30]. Wildy, Goad & Allen [50] argue that this result seems to favour the clumpy model over the homogeneous scenario as it could be due to an outflow in which the greater column density of C IV ions over Si IV means that C IV is more likely to be saturated.

The velocities in which variability occurs span a quite wide range. In the case of J101056.69+355833.3 we have: C IV varies in the lowest (∼-3900 km s^{-1}) as well as in the highest (∼-12440 km s^{-1}) velocity component. On the contrary, Si IV varies in the first four low velocity components (∼-3900, ∼-4700, ∼-5570 ∼-6350 km s^{-1}) as well as in two high velocity components (∼-9120, ∼-10050 km s^{-1}). In the case of J114548.38+ 393746.6 the situation is as follows: C IV varies only in two higher velocity components (∼-7600, ∼-6900 km s^{-1}). In contrast, Si IV doesn't show any variation in the higher velocity components. Instead, variability occurs in velocities ranging from ∼-4800 up to ∼-6400 km s^{-1}.

By comparing Si IV and C IV variable components at the same velocity shifts we observe no correlations, except for one case in J101056.69+355833.3. More specific, the lower velocity components of C IV and Si IV (at ∼-3900 km s^{-1}) have both varied and in the same sense i.e. they both became weaker. If C IV and Si IV had the same covering fraction, then we would expect the incidence of variability in C IV to be the same as that of Si IV which is contradicted by our results. So it is more possible that C IV and Si IV have different covering fractions [65–71]. Indeed, Si IV can have a smaller covering fraction than C IV. If Si IV is tracing a smaller area of the gas cloud than C IV and this cloud is moving across our line-of-sight, then Si IV absorption would generally be more variable [30]. Furthermore, if C IV and Si IV indeed have different covering fractions then the change in covering fraction, as well as the change in EW of the absorption lines, for each ion can also differ. Finally, we need to point out that Capellupo et al. [30] in their sample found that ∼50% of the variable Si IV regions did not have corresponding C IV variability at the same velocities while nearly almost every variable C IV had corresponding changes in Si IV. From our analysis we cannot conclude to a reliable result since our sample of two BALQSOs is only indicative.

The fact that only individual components vary, favours the scenario where the movement of individual clouds or substructures in the outflow, across our line of sight, is the reason of the observed variability. The movements of individual clouds indicate changes in the covering factor. These results are in agreement with Lundgren et al. [27],

Table 4. Top: values of $N_\sigma(\lambda)$ for the 9 components of the blue and the red lines of the C IV and Si IV doublets for the two spectra of J101056.69+355833.3, taken on 19/01/2005 (SDSS) and on 08/02/2011 (BOSS).Bottom: values of $N_\sigma(\lambda)$ for the 10 components of the blue and the red lines of the C IV and Si IV doublets for the two spectra of J114548.38+393746.6, taken on 13/03/2005 (SDSS) and on 08/04/2011 (BOSS).

J101056.69+355833.3					
Component	Velocity (km s^{-1})	$N_\sigma(\lambda)$ for C IV		$N_\sigma(\lambda)$ for Si IV	
		blue	red	blue	red
1	-3900	1.46	1.59	1.58	1.58
2	-4740	0.23	0.34	1.30	1.22
3	-5570	0.97	0.41	-1.19	-1.08
4	-6350	0.00	-0.59	-1.09	-1.30
5	-7360	0.93	-0.89	0.90	-0.19
6	-8260	0.16	-0.69	-0.34	-0.92
7	-9120	0.36	0.33	-1.64	-1.73
8	-10050	-0.45	-0.08	-2.03	-1.73
9	-12440	-2.19	-1.87	0.00	0.00

J114548.38+393746.6					
Component	Velocity (km s^{-1})	$N_\sigma(\lambda)$ for C IV		$N_\sigma(\lambda)$ for Si IV	
		blue	red	blue	red
1	-1840	-0.16	-0.16	-0.76	0.48
2	-2950	0.00	0.00	0.00	0.00
3	-4310	-0.10	-0.48	0.00	0.00
4	-4830	-0.06	0.53	-1.32	-1.15
5	-5280	-0.23	0.00	-1.12	-2.42
6	-5740	0.00	0.00	-2.30	-2.30
7	-5960	0.56	0.06	-1.29	-1.41
8	-6430	0.00	-0.09	-1.55	-1.08
9	-6870	-1.88	-1.03	-1.08	0.00
10	-7650	-2.58	-2.51	0.13	0.13

Gibson et al. [44] and Capellupo et al. [30]. In general, changes in ionization would result in more global changes in a BAL trough rather than changes in individual components of the trough.

One more piece of evidence favouring the crossing cloud scenario comes from the observation that within the same BAL trough some components strengthen while others weaken. This is obvious in J101056.69+355833.3. In C IV the component at $\sim$ -3900 km s^{-1} weakens while the component at $\sim$-12500 km s^{-1} becomes stronger. In SiIV, the components at $\sim$-3900 km s^{-1} and $\sim$-4700 km s^{-1} weaken while the components at $\sim$-5600 km s^{-1}, $\sim$-6400 km s^{-1}, $\sim$-9100 km s^{-1} and $\sim$ -10000 km s^{-1} strengthen over time. This can be explained in a moving cloud scenario, as one cloud might enter our line of sight while another is leaving it. On the other hand in the second BALQSO, J114548.38+393746.6, we observe coordinated variabilities between absorption components at different velocities within the same BAL trough. This takes place both in C IV and in Si IV. This fact favours changing ionization of the outflowing gas as the cause of variability. In order to support the crossing cloud scenario one should require coordinated cloud movements at different outflow velocities and radii, which seems unlikely [30].

However, there is a contradiction which appears at this point. In the second BALQSO (J114548.38+393746.6) where ionization changes seem to cause variability, the C IV and Si IV BELs (Broad Emission Lines) did not vary at all. As we know the ionization of C IV and Si IV BELs is controlled by the same far-UV flux that controls the C IV and Si IV absorption lines. Changes in quasar continuum fluxes are known to cause changes in the BELs after a time lag related to the light travel time between the continuum source and the BEL region [45]. In the case of J101056.69+355833.3, where the cloud scenario is more possible, we observe variability in both C IV Si IV BELs. This contradiction leads us to support a complicated scenario where both changes in covering factor and ionization changes are responsible for BAL variability. This point of view is supported by the findings of Capellupo et al. [30] who were the first that proposed this interpretation.

It is extremely important to note that the results concerning the variability of BAL troughs, in general, should be treated with caution as our sample consists of only two BALQSOs from two different epochs.

6 Conclusions

Using the model of Danezis et al. [52–54], Lyratzi et al. [11, 55] and the fitting criteria and physical model proposed by Stathopoulos et al. [18] we decompose the broad absorp-

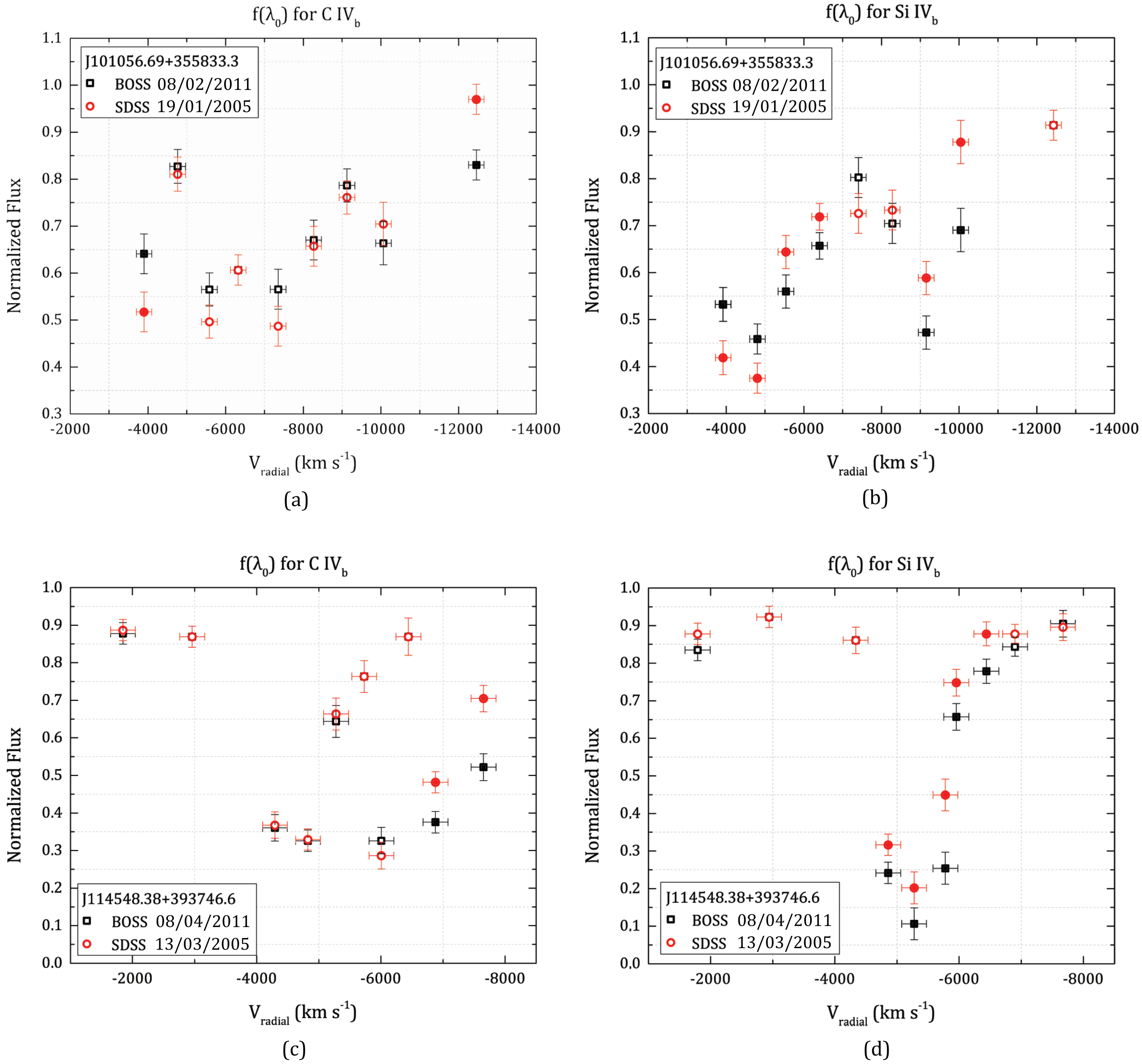

Fig. 3. Top: line flux at line center for the blue components of C IV (a) and Si IV (b) between two epochs for J101056.69+355833.3. Bottom: line flux at line center for the blue components of C IV (c) and Si IV (d) between two epochs for J114548.38+393746.6. Circles corrspond to the SDSS spectra, while squares correspond to the BOSS spectra. Note that the filled circles and filled squares denote the variable components between BOSS and SDSS spectra.The red components of C IV and Si IV for both BALQSOs follow the same trends as the blue components.

tion troughs of two BALQSOs into the individual components they consist of. We show that BAL troughs are the product of structures in the wind we call "clouds" and not the product of a smooth continuous flow. By analyzing a BAL trough to its components we have the advantage to study the variations of the individual absorbing systems in the line of sight and not just the variations of the whole absorption trough. We find no evidence indicating acceleration or de-acceleration of the absorbing systems in the line of sight. The FWHMs of the individual components do not vary between a period of six years indicating that the structure and/or internal velocity field of the absorbers remains constant.

All variable components show changes in the optical depths at line centers which are also manifested as variations in the EW of the components. In both BALQSOs, over corresponding velocities Si IV has higher incidence of variability than C IV. This result is usually interpreted in terms of line strengths, as the Si IV BALs are generally weaker than C IV BALs and weaker lines tend to be more variable [30]. Furthermore, this result seems to favour the clumpy model over the homogeneous scenario as it could be due to an outflow in which the greater column density of C IV ions over Si IV means that C IV is more likely to be saturated.

We found no correlations between Si IV and C IV variable components at the same velocity shifts, except for one single case. This result points towards different covering fractions between Si IV and C IV. If both ions had the same covering factor we would expect to observe the same incidence of variability.

In both BALQSOs and both ions, variability occurs only in individual components which favours the crossing cloud scenario over chancing ionization, as the driver of BAL variability.

Although most of our results favour the crossing cloud scenario as the cause of variability, there is also strong piece of evidence indicating variability driven by changes in ionization. In J114548.38+393746.6 we observe coordinated variability within the same BAL troughs, which occurs in both ions. Furthermore, in J101056.69+355833.3, which shows strong evidence favouring the crossing cloud scenario, the BELs of Si IV and C IV exhibit strong variability. On the other hand, in J114548.38+393746.6 we observe the exact opposite i.e. evidence favouring ionization changes but no variability in Si IV and C IV BELs. We remind that changes in quasar continuum fluxes are known to cause changes in the BELs after a time lag. Thus, we conclude that a mixed situation where both physical mechanisms contribute to BAL variability, is the most possible scenario.

We need to point out that our sample of two BALQSOs is very small. So, unless we study a larger sample and investigate the correlation between variability and continuum variations we cannot draw any general conclusions about the variability of Si IV and C IV broad absorption troughs. To conclude, we point out that in order to fit broad absorption trough we firstly fit the broad emission lines. The results of the analysis of BELs as well as the correlations with BALs will be presented in a future work.

7 Acknowledgements

This research project is progressing under the financial support of the Ted and Erica Spyropoulos Foundation and the Special Account for Research Grants of University of Athens, which we thank very much.

8 Author contribution statement

This paper is a first approach in a variability study of Si IV and C IV BALs in sample of BALQSOs. The variability study is a part of the thesis of the PhD candidate D. Stathopoulos. The purpose of this study is to investigate the reasons of variability observed in the Si IV and C IV BALs of quasars.

This PhD thesis, is a part of a series of theses and a more general research project under the supervision of Dr. E. Danezis, leader of the Astrophysical Spectroscopy Team of the National and Kapodistrian University of Athens. All authors of this paper, are members of the research team which is active since 1984. Our research interests, among others, involve UV spectroscopy of Hot Stars, Wolf Rayet Stars, Cataclysmic Variables and Quasars. As a result, all authors have contributed in this paper in the following ways: (a) inspecting the Si IV and C IV fits in both BALQSOs, (b) during the process of data reduction, (c) checking the results obtained from the fitting process, (e) discussing the problems that arose and suggesting possible solutions, (f) discussing the results and reaching to conclusions.

From a technical point of view, Dr. D. Tzimeas and D. Stathopoulos cooperate in order to improve and provide extensions to our spectral analysis software which is based on the model constructed by our research group. Finally, Dr. E. Danezis, Dr, E. Lyratzi and Dr. A. Antoniou focus on the theoretical background of the software.

References

1. Reichard, T. A. et al., AJ **126**, (2003) 2594.
2. Hewett, P. C., Foltz, C. B., AJ, **125**, (2003), 1784.
3. Hall, P.B., et al., MNRAS, **434**, (2013), 222.
4. Weymann R. J., Morris S. L., Foltz C. B., Hewett P. C., ApJ, **373**, (1991), 23.
5. Foltz, C., Wilkes, B., Weymann, R, Turnshek, D., PASP, **95**, (1983), 341.
6. Turnshek, D. A., *QSO Absorption Lines: Probing the Universe* (ed. J. C. Blades, D. A., 1988).
7. Scargle, J. D., Caroff, L. J., Noerdlinger, P. D., Ap.J (Letters), **161**, (1970), 115.
8. Murray N., Chiang J., Grossman S. A., Voit G. M., ApJ, **451**, (1995), 498.
9. McKee, C. F. & Tarter, C. B., ApJ, **202**, (1975), 306.
10. Turnshek, D. A., ApJ, **280**, (1984), 51.
11. Lyratzi, E., Popović, L. Č., Danezis, E., Dimitrijević, M. S., & Antoniou, A., NewAR, **53**, (2009), 179.
12. Lyratzi, E., Danezis, E., Popović, L. Č., Dimitrijević, M. S., Antoniou, A. & Stathopoulos, D., MSAIS, **15**, (2010), 161.
13. Lyratzi, E., Danezis, E., Popović, L. Č., Antoniou, A., Dimitrijević, M. S., & Stathopoulos, D., BaltA, **20**, (2011), 448.
14. Hamann, F., Chartas, G., McGraw, S., Rodriguez Hidalgo, P., Shields, J., Capellupo, D., Charlton, J. & Eracleous, M., MNRAS, **435**, (2013), 133.
15. Takeuchi, S., Ohsuga, K. & Mineshige, S., PASJ, **65**, (2013), 88.
16. Capellupo, D. M., Hamann, F. & Barlow, T. A., MNRAS, **444**, (2014), 1893.
17. Misawa, T., Inada, N., Oguri, M., Gandhi, P., Horiuchi, T., Koyamada, S. & Okamoto, R., ApJ, **794**, (2014), 20.
18. Stathopoulos, D., Danezis, E., Lyratzi, E., Antoniou, A., Tzimeas, D., JApA, **36**, (2015), 495.
19. Matthews, J. H., Knigge, C., Long, K. S., Sim, S. A., Higginbottom, N., Mangham, S. W., MNRAS, **458**, (2016), 29.

20. Waters, T., Proga, D., MNRAS, **460**, (2016), 79.
21. Mathews, W. G., ApJ, **189**, (1974), 23.
22. Krolik, J., McKee, C. M., & Tarter, C. B., ApJ, **249**, (1981), 422.
23. Bottorff, M. & Ferland, G. ApJ, **549**, (2001), 118.
24. Hamann F., Barlow T. A., Junkkarinen V., ApJ, **478**, (1997), 87.
25. Srianand R., Petitjean P., A&A, **373**, (2001), 816.
26. Misawa T., Eracleous M., Charlton J. C., Tajitsu A., ApJ, **629**, (2005), 115.
27. Lundgren B. F., Wilhite B. C., Brunner R. J., Hall P. B., Schneider D. P., York D. G., Vanden Berk, D. E., Brinkmann J., ApJ, **656**, (2007), 73.
28. Hall P. B., Anosov K., White R. L., Brandt W. N., Gregg M. D., Gibson R. R., Becker R. H., Schneider D. P., MNRAS, **411**, (2011), 2653.
29. Capellupo D. M., Hamann F., Shields J. C., Halpern J., Hidalgo P. R., Barlow T. A., *Astronomical Society of the Pacific Conference Series, AGN Winds in Charleston, eds. Chartas G., Hamann F., Leighly K. M., 2012*, **460**, 88.
30. Capellupo D. M., Hamann F., Shields J. C., Rodriguez Hidalgo P., Barlow T. A., MNRAS, **422**, (2012), 3249.
31. Capellupo D. M., Hamann F., Shields J. C., et al., MNRAS, **429**, (2013), 1872.
32. Filiz Ak N., Brandt W. N., Hall P. B., Schneider D. P., Anderson S. F., Hamann F., Lundgren B. F., Myers A. D., Paris I., Petitjean P., Ross N. P., Shen Y., York D., ApJ, **777**, (2013), 168.
33. Vivek M., Srianand R., Petitjean P., Mohan V., Mahabal A., Samui S., MNRAS, **440**, (2014), 799.
34. Hamann F., Kaplan K. F., Rodriguez Hidalgo P., et al., MNRAS (Letters), **391**, (2008), 39.
35. Rodriguez Hidalgo P., Hamann F., Hall P., MNRAS, **411**, (2011), 247.
36. Vivek M., Srianand R., Mahabal A., Kuriakose V. C., MNRAS, (Letters) **421**, (2012), 107.
37. Vivek M., Srianand R., Petitjean P., Noterdaeme P., Mohan V., Mahabal A., Kuriakose V. C., MNRAS, **423**, (2012), 2879.
38. Wildy C., Goad M. R., Allen J. T., MNRAS, **448**, (2015), 2397.
39. Gabel J. R. et al., ApJ, **595**, (2003), 120.
40. Hall P. B., Sadavoy S. I., Hutsemekers D., Everett J. E., Rafiee A., ApJ, **665**, (2007), 174.
41. Capellupo D. M., Hamann F., Shields J. C., Rodriguez Hidalgo P., Barlow T. A., MNRAS, **413**, (2011), 908.
42. Barlow T. A., *PhD thesis*, AA(California Univ., 1993).
43. Wise J. H., Eracleous M., Charlton J. C., Ganguly R., ApJ, **613**, (2004), 129.
44. Gibson R. R., Brandt W. N., Schneider D. P., Gallagher S. C., ApJ, **675**, (2008), 985.
45. Hamann, F. MNRAS, **391**, (2008), 39.
46. Gibson R. R., Brandt W. N., Gallagher S. C., Hewett P. C., Schneider D. P., ApJ, **713**, (2010), 220.
47. Barlow T. A., Junkkarinen V. T., Burbidge E. M., Weymann R. J., Morris S. L., Korista K. T., ApJ, **397**, (1992), 81.
48. Misawa, T., Eracleous, M., Charlton, J. C.,&Kashikawa, N., ApJ, **660**, (2007), 152.
49. Welling, C. A., Miller, B. P., Brandt, W. N., Capellupo, D. M., Gibson, R. R., MNRAS, **440**, (2014), 2474.
50. Wildy C., Goad M. R., Allen J. T., MNRAS, **437**, (2014), 1976.
51. He, Z.-C., Bian, W. -H., Ge, X., Jiang, X.-L., MNRAS, **454**, (2015), 3962.
52. Danezis, E., Nikolaidis, D., Lyratzi, V., Stathopoulou, M., Theodossiou, E., Kosionidis, A., Drakopoulos, C., Christou, G. & Koutsouris, P., Ap&SS, **284**, (2003), 1119.
53. Danezis, E., Nikolaidis, D., Lyratzi, E., Popović, L. Č., Dimitrijević, M. S., Antoniou, A. & Theodosiou E., PASJ, **59**, (2007), 827
54. Danezis, E., Lyratzi, E., Popović, L. Č., Dimitrijević, M. S., Antoniou, A., NewAR, **53**, (2009), 214
55. Lyratzi, E., Danezis, E., Popović, L. Č., Dimitrijević, M. S., Nikolaidis, D. & Antoniou, A., PASJ, **59**, (2007), 357.
56. Markova, N., A&AS, **144**, (2000), 391.
57. Bates, B. & Gilheany, S. MNRAS, **243**, (1990), 320.
58. Gilheany, S. et al., Ap&SS, **169**, (1990), 85.
59. Waldron, W. L., Klein, L., & Altner B., *ASP Conf. Series* (1992) **22**, 181.
60. Rivinius, T. et al., A&A, **318**, (1997), 819.
61. Danezis, E., *The nature of Be stars, (PhD thesis)*, (University of Athens, 1983).
62. Fitzpatrick, E.L., & Massa, D.L., ApJ, **525**, (1999), 1011.
63. Schlegel, D. J., Finkbeiner, D. P., & Davis, M., ApJ, **500**, (1998), 525.
64. Rafiee, A. & Hall, P. B., ApJS, **194**, (2011), 42.
65. Barlow T. A., Sargent W. L. W., AJ, **113**, (1997), 136.
66. Hamann F., Barlow T. A., Junkkarinen V., Burbidge E. M., ApJ, **478**, (1997), 80.
67. Hamann F. W., Barlow T. A., Chaffee F. C., Foltz C. B., Weymann R. J., ApJ, **550**, (2001), 142.
68. Ganguly R., Eracleous M., Charlton J. C., Churchill C.W., AJ, **117**, (1999), 2594.
69. Gabel J. R., Arav N., Kaastra J. S., Kriss G. A., Behar E., Costantini E., Gaskell C. M., Korista K. T., Laor A., Paerels F., Proga D., Quijano J. K., Sako M., Scott J. E., Steenbrugge K. C., ApJ, **623**, (2005), 85.
70. Gabel J. R., Arav N., Kim T.-S., ApJ, **646**, (2006), 742.
71. Arav N., Moe M., Costantini E., Korista K. T., Benn C., Ellison S., ApJ, **681**, (2008), 954.